

Gate Sequence Optimization for Parameterized Quantum Circuits using Reinforcement Learning

Tom R. Rieckmann, Stefan Scheel, and A. Douglas K. Plato

Institute for Physics, University of Rostock, Albert-Einstein-Straße 23-24, 18059 Rostock, Germany

Current experimental quantum computing devices are limited by noise, mainly originating from entangling gates. If an efficient gate sequence for an operation is unknown, one often employs layered parameterized quantum circuits, especially hardware-efficient ansätze, with fixed entangling layer structures. We demonstrate a reinforcement learning algorithm to improve on these by optimizing the entangling gate sequence in the task of quantum state preparation. This allows us to restrict the required number of CNOT gates while taking the qubit connectivity architecture into account. Recent advancements using reinforcement learning have already demonstrated the power of this technique when optimizing the circuit for a sequence of non-parameterized gates. We extend this approach to parameterized gate sets by incorporating general single-qubit unitaries, thus allowing us to consistently reach higher state preparation fidelities at the same number of CNOT gates compared to a hardware-efficient ansatz.

1 Introduction

Quantum computing has made major advancements in recent years, with multiple systems claiming to have reached quantum primacy [1–3]. However, these results have been achieved on artificial problems such as random circuit sampling [4] without any known ‘real world’ applications. Current systems still fall short of being able to perform the tasks at the heart of quantum computing development such as Shor’s algorithm [5, 6], quantum simulation [7], and quantum machine learning [8]. While the recent experimen-

Tom R. Rieckmann: tom.rieckmann@uni-rostock.de

tal demonstrations of error correction are promising [9], a full scale implementation is still out of reach for today’s noisy intermediate-scale quantum (NISQ) systems [10].

Consequently, there is a strong interest in finding algorithms that can yield useful results without the need for fault tolerance through error correction [10, 11]. Recent work on large interacting systems, where classical approaches struggle, have demonstrated methods for calculating expectation values [12] and ground state energies [13]. However, noise is still a major limiting factor for the maximally viable scale of the calculations and one requires error mitigation techniques to get meaningful results on current devices. These techniques, such as zero noise extrapolation or readout error mitigation, rely on postprocessing of repeated circuit evaluations to improve the directly measured results [14]. Instead, one of the most obvious paths to avoiding noise is to optimize the algorithm’s quantum circuit. This requires defining a useful optimization target. Our main goal is to minimize the number of entangling gates, as for most experimental systems these are the dominant source of errors [15]. We expect that, as a by-product, the depth of the circuit is also kept small, which is particularly important for systems with short dephasing and relaxation times compared to the gate execution time, such as is the case with superconducting qubits.

Optimization of circuits is a well-known task with tools provided by many quantum computing frameworks [16, 17]. However, such methods can be computationally expensive, with recent work suggesting that most quantum circuit optimization problems are NP-hard [18, 19]. Finding efficient implementations is particularly difficult when the exact unitary to be implemented is not yet fully determined by a gate sequence, as is the case for variational quantum algorithms [20], such as variational quantum eigensolvers [21, 22]

and quantum machine learning [23, 24]. One approach is to make use of parameterized quantum circuits, where the general structure is fixed, but variable gates, such as angle-dependent rotations, allow for control over the output distributions. This relies on finding an ansatz with sufficient expressibility for all desired operations.

A variety of gate sequences have been proposed, which can implement any unitary or state by varying only their continuous parameters, and lower bounds for the minimally required number of entangling gates for this task have been determined [25–28]. More recently, circuits created by repeating layers of local gates and layers of a fixed entangling gate sequence to approximate any desired operation have become popular. They can significantly reduce the gate number, while still being highly expressive in the types of operations they can represent [29, 30]. Even though this one-size-fits-all approach is very simple to use and yields good results, it is by no means optimal, particularly when considering the properties and limitations of individual experimental systems.

Instead, we propose a reinforcement learning (RL) algorithm to optimize the entangling gate sequence for a parameterized universal gate set, and apply it to the problem of quantum state preparation. RL has previously been applied to optimizing circuits, initially limited to the Clifford gate set [31, 32], as well as unitary synthesis [33]. Current research has taken a focus on the discrete Clifford+T gate set [34, 35]. These works have demonstrated that such algorithms can generalize to the entire problem space from only a limited number of training simulations while taking CNOT connectivity architectures into account. Our work differs by including arbitrary parameterized single-qubit gates, which makes our gate set more similar to the native gate set employed on many experimental systems, such as those developed by IBM [16]. This allows us to investigate the effectiveness of RL for optimizing circuits used in variational quantum algorithms.

In this paper, we will first introduce the theoretical background and experimental limitations for quantum state preparation. We then detail the design of the RL agent. Results are compared to layered parameterized circuits with common hardware-efficient entangling sequences. In our analysis we have placed the focus on the properties of publicly available quantum computers

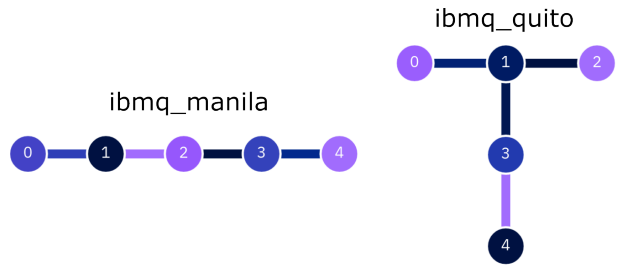


Figure 1: CNOT connectivity for `ibmq_manila` and `ibmq_quito`. Numbers represent qubits, connections depict CNOTs connections in the hardware. The colour coding is given by gate errors (connections) and decoherence (qubits). Images taken from IBM Quantum [16].

from IBM, but the general approach can be deployed on any system using a gate-based computation model.

2 Optimal Quantum State Preparation

In quantum state preparation, the goal is to achieve a target $|\psi_T\rangle$ starting from the initial state of the experimental system (usually the n -qubit computational basis state $|0\rangle$). With a universal quantum gate set, an exact solution for this task is guaranteed to exist when neglecting noise [36, 37].

On NISQ devices noise cannot be ignored, thus any state preparation will not be exact. To quantify the accuracy we use the fidelity

$$F(\rho, \sigma) = \left(\text{tr} \left(\sqrt{\rho^{1/2} \sigma \rho^{1/2}} \right) \right)^2, \quad (1)$$

which simplifies to $F(\rho, |\psi\rangle) = \langle \psi | \rho | \psi \rangle$ if one of the states is pure [37].

While entangling gates, such as the CNOT gate, generally have the biggest impact on fidelity, additional care has to be taken when constructing the circuit to consider the architecture of the specific device. Due to experimental limitations, one cannot choose any pair of qubits as control and target.

2.1 Gate Set Limitations

Entangling gates that are directly implementable on hardware are determined by the system’s qubit connectivity architecture. CNOT gate connectivity examples for two previous IBM Quantum systems can be seen in Figure 1. For the remainder of this paper we will restrict entanglement operations to CNOT gates, though all statements

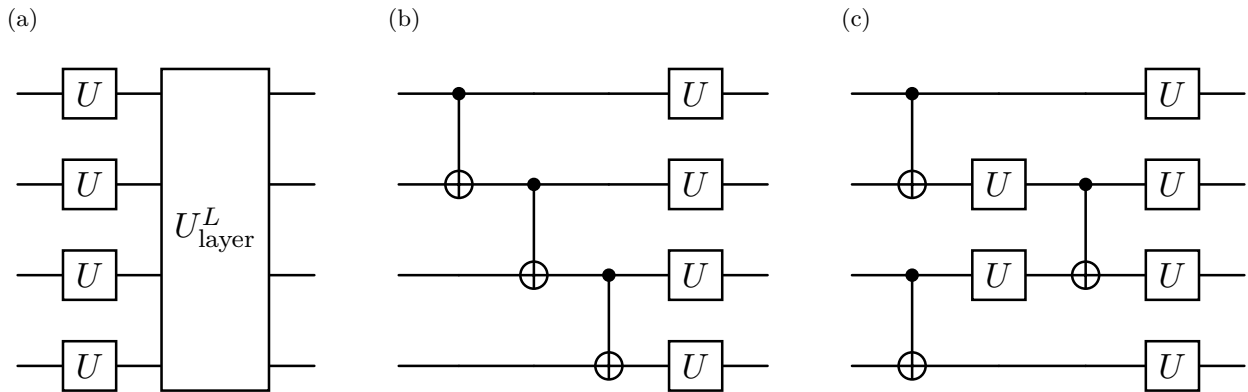


Figure 2: Makeup of a layered parameterized circuit. Single-qubit gates U are parameterized with up to three independent parameters each. (a) depicts the general structure, which consists of layers U_{layer} repeated L times. As layers begin with entangling gates, a local rotation layer is added at the beginning. In (b) (linear layer) and (c) (pairwise layer) one can see two popular variants for U_{layer} , which will be used for the performance comparison of our algorithm.

regarding its properties and usage can also be applied to equivalent¹ entangling gates such as the ECR gate [16].

Circuits that make use of gates not directly available on the device have to be mapped to the architecture. The most direct approach is to use SWAP gates, which each contain up to 3 CNOTs. While more sophisticated approaches, such as those implemented in the IBM transpiler [16], may yield much better results, these mapping procedures should be avoided during circuit design. This becomes even more important for larger circuits with respect to depth and width, as the likelihood for an efficient relabelling of qubits decreases.

2.2 Layered Parameterized Circuits

Hardware-efficient ansätze are designed to avoid these transpiling issues by densely stacking CNOT gates in a nearest neighbour architecture. This forms an entangling layer U_{ent} , which is interleaved with local rotation layers U_{rot} . In [29] a variety of different entangling layers were compared in terms of their expressibility and entangling capability. Examples for two of the most popular structures can be seen in Figure 2. By stacking enough layers $U_{\text{layer}} = U_{\text{rot}}(\boldsymbol{\theta})U_{\text{ent}}$, uni-

versality of an ansatz is guaranteed. A unitary is implemented by

$$U = \left(\prod_l^L U_{\text{rot}}(\boldsymbol{\theta}_l) U_{\text{ent}} \right) U_{\text{rot}}(\boldsymbol{\theta}_0), \quad (2)$$

with

$$U_{\text{rot}} = U_{\text{local}}^{\otimes n}. \quad (3)$$

Often

$$U_{\text{local}}(\theta_1, \theta_2) = R_z(\theta_1)R_y(\theta_2) \quad (4)$$

is sufficient instead of an arbitrary single-qubit rotations, as Eq. (4) can reach any possible output provided that one does not start in an eigenstate of R_y . The free parameters of each local rotation layer $\boldsymbol{\theta}_l$ are determined using classical optimization methods. Optimization techniques designed for parameterized quantum circuits, such as quantum natural gradient, may converge in fewer steps than standard gradient descent or ADAM [38].

3 Method

While the layered parameterized circuit approach has proven successful, it requires significant redundancy in the number of gate operations in order to express a wide range of quantum states. In addition, the choice of layer structure is also limited by the available hardware architecture. Both these issues can be overcome by employing an adaptive circuit design strategy, where an

¹We consider the entangling gates equivalent if one can be derived from the other by only adding single qubit rotations before and after. Our algorithm can be used identically by simple replacing the CNOT gates after the fact and simplifying neighbouring single qubit rotations.

Algorithm 1: Circuit Generation

Data: Target ρ_T , empty circuit C , agent (NN, outputs Q_W), state loss L , maximum number of actions M

Result: Populated circuit C

Add local rotation layer $U_{\text{rot}}(\boldsymbol{\theta}_0)$ to C

Minimize $L(U_{\text{rot}}\rho_T U_{\text{rot}}^\dagger)$ to determine $\boldsymbol{\theta}_0$

Find $\rho_1 = U_{\text{rot}}\rho_T U_{\text{rot}}^\dagger$

for $k = 1, 2, \dots, M$ **do**

 Observe input \mathbf{v}_{in} from ρ_k of s_k

 Get state-action values $\mathbf{Q}_W(s_k, a)$ from NN using \mathbf{v}_{in} as input

 Sample a_k from $\mathbf{Q}_W(s_k, a)$

if a_k is stop **then**

 Set $N = k - 1$

 break

end

 Get U_k from U_{CX} of chosen CNOT and U_{local} on control, target qubits

 Minimize $L(U_k(\boldsymbol{\theta}_k)\rho_k U_k^\dagger(\boldsymbol{\theta}_k))$ over $\boldsymbol{\theta}_k$

 Set $\rho_{k+1} = U_k \rho_k U_k^\dagger$

end

Full Circuit C defines U_C

Minimize $L(U_C \rho_T U_C^\dagger)$ to redetermine all $\boldsymbol{\theta}_0, \boldsymbol{\theta}_1, \dots, \boldsymbol{\theta}_N$ in $U_C(\boldsymbol{\theta}_0, \boldsymbol{\theta}_1, \dots, \boldsymbol{\theta}_N)$

Add NOT gates to go from closest computational basis state $|b\rangle$ to $|0\rangle$

Invert circuit for state preparation task with $\rho_{\text{final}} = U_C^\dagger |0\rangle\langle 0| U_C$

algorithm first determines an optimal gate structure, before standard optimisation techniques are used to fix the continuous gate parameters. This problem is particularly suited to reinforcement learning (RL), as it does not require a priori representative datasets of known efficient quantum circuits – which are computationally expensive to generate. Our approach is based on a Double Deep Q-Network (DDQN) agent [39], which builds circuits sequentially by selecting two-qubit operations (actions) using an evaluation by a neural network (NN). At every step, k , in the circuit generation process, we can choose to either stop (if the circuit is deemed to be complete), or apply a parameterizable two-qubit gate drawn from a predetermined allowable gate set. Our goal is achieving an arbitrary target state with as few entanglement operations as possible. For practical reasons we consider the inverse problem of transforming a target state back to the ground

state, as this simplifies the optimization and evaluation. The objective then becomes finding a policy, which at each step chooses the action which is most likely to lead to the ground state in the least number of overall steps. Note, this need not be the action with the best immediate improvement.

The process of circuit generation from a trained NN is explained in Section 3.1, with a summary given by Algorithm 1. Section 3.2 provides a detailed description of our agent. Training parameters can be found in [40] or by reaching out to the authors.

3.1 Circuit Generation

The neural network evaluation requires a (real) vector input containing information about the current state of the system, s_k . As we are working with the inverse problem, we do not need to provide ρ_T at each step, and instead only keep track of the current density matrix, ρ_k , along with an optional list of previously applied actions, $\{a_j\}_{j < k}$. Thus, we construct the NN input at step k as,

$$\mathbf{v}_{\text{in}}(s_k) = \begin{pmatrix} \text{vec}(\rho_k - \frac{\mathbb{I}}{d}) \\ c_{\text{in}} \text{key}(a_0) \\ \vdots \\ c_{\text{in}} \text{key}(a_{k-1}) \\ 0 \\ \vdots \end{pmatrix}, \quad (5)$$

where the vectorisation is over the real and imaginary parts of $\rho_k - \frac{\mathbb{I}}{d}$, d is the dimension of the Hilbert space and $\text{key}(a)$ are zero mean vectors uniquely identifying each possible action, constructed from a binary representation of the NN output vector index associated to that action. The subtraction of a trace one matrix from ρ_k , together with the normalisation of the action keys, ensures that, in accordance with standard data preprocessing procedures [41], each feature has an expected mean of zero over datasets of Haar random states. We also introduce a scaling factor c_{in} , set during training, which determines the relative importance given to past actions vs. the current density matrix (its role will be described in more detail in Section 3.2). Finally, to maintain constant input dimensions, the input vector is padded with zeros corresponding to future actions.

The objective of the algorithm is to find a gate sequence which diagonalises the target density

matrix in the computational basis. From this one can readily reach the ground state, $|0\rangle$, by appropriate application of Pauli X operations to relevant qubits. Thus, a suitable loss function for determining gate parameters is given by,

$$L(\rho) = \sum_i \sum_{j=i+1} |\rho_{ij}|^2, \quad (6)$$

which can be minimised using the Broyden–Fletcher–Goldfarb–Shanno (BFGS) algorithm. The initial data for the NN input is determined by first applying a layer of parameterized local unitaries, U_{rot} , to the n qubit target state ρ_T , and then minimising $L(U_{\text{rot}}\rho_T U_{\text{rot}}^\dagger)$ to obtain ρ_1 . This provides $\mathbf{v}_{\text{in}}(s_1)$. The sequence of entangling gates is then determined by repeatedly applying unitaries corresponding to actions a_k sampled from our RL agent, updating \mathbf{v}_{in} at each step. The sampling process makes use of the NN output vector, which is trained (see Section 3.2) to provide an estimate of the exact state-action values Q_{true} defined by,

$$Q_{\text{true}}(s_k, a_k) = r_k + \gamma V_{\text{true}}(s_{k+1}), \quad (7)$$

where r_k is the reward signal. V_{true} represents the value/desirability of the next state and $\gamma < 1$ is the discount factor, which can be tuned to make the agent prioritize short episodes. In the final state s_N of an episode, the state-action value is $Q_{\text{true}}(s_k, a_k) = r_k$.

The optimal strategy maximizing future rewards is the one that always picks the action a_k with the highest "true" state-action value. Under this policy $V_{\text{true}}(s_{k+1}) = \max_a Q_{\text{true}}(s_{k+1}, a)$, i.e.

$$Q_{\text{true}}(s_k, a_k) = r_k + \gamma \max_a Q_{\text{true}}(s_{k+1}, a) \quad (8)$$

$$= \sum_{l=k}^N \gamma^{l-k} r_l. \quad (9)$$

Note that $\mathbf{Q}(s_k, a)$ represents a d_{out} -dimensional vector containing the values of all actions in state s_k , and a_k represents a specific action associated to an entry of this vector. Thus $Q(s_k, a_k)$ and $\max_a Q(s_{k+1}, a)$ are scalar. For a given architecture, we set d_{out} to the total number of allowable CNOT gates plus one (for the stopping action), though in principle additional gate combinations could be included. Thus each action a_k is mapped to a unitary $U_k \equiv U_{a_k}$ composed of a CNOT gate, U_{CX} , which we then append with local parameterized unitaries on the control and target qubits

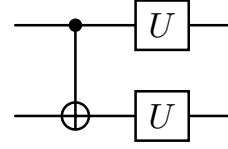


Figure 3: Individual action which we use for our results. Local gates are only added on target and control qubits of an entangling gate. Other single-qubit operations or entangling gates may be chosen as elementary building blocks, such as the Toffoli gate or the controlled-Z gate.

in order to guarantee universality (Fig. 3). The set of all continuous gate parameters for the action are collectively labelled θ_k and determined at each step by minimizing the loss, Eq. (6), using the BFGS algorithm, which yields the next $\rho_{k+1} = U_k(\theta_k)\rho_k U_k^\dagger(\theta_k)$.

With only such local optimizations, the generated circuits are typically inefficient in terms of their gate number, as the optimal gate parameters are dependent on the future gate sequence. To account for this, the final state is determined by performing a global minimization of (6) over all continuous parameters, once the complete gate sequence has been established. A comparison of the performance with and without global optimization is given in Table 1. Due to its high computational cost, we perform this minimization only once after the entire gate sequence has been determined. The state preparation can then easily be performed using the inverse circuit, which should yield states as accurate to ρ_T as possible. By evaluating the circuit with a reward r_k proportional to the fidelity between the final state ρ_{final} and the target ρ_T combined with a discount $\gamma < 1$, we can create an environment where the agent is not only focused on maximizing the fidelity, but also on finding the shortest gate sequence to do so.

Finally, to guarantee the desired accuracy, we add a fidelity threshold T_F , which must be reached in order to receive a reward

$$r_k(s_k) = \begin{cases} c_r F(\rho_{\text{final}}, \rho_T) & \text{if } k = N \\ & \& 1 - F < T_F \\ 0 & \text{else.} \end{cases} \quad (10)$$

Actions during the episode receive no reward or penalty. c_r is a simple scaling factor. In practice, the final step reward r_N can more easily be

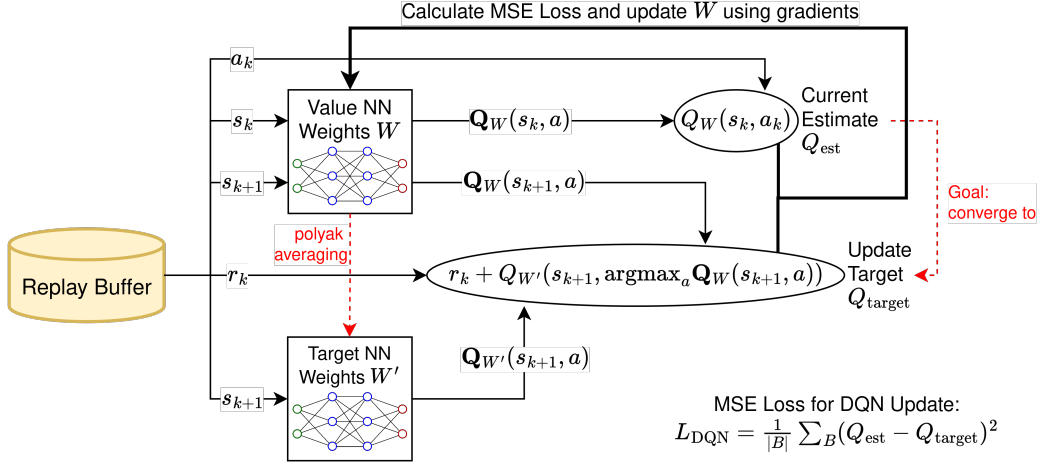


Figure 4: Schematic depicting the process of updating the NN weights from data stored in the replay buffer. The procedure is not performed for a single set of (s_k, a_k, r_k, s_{k+1}) but rather for a batch B . The target NN is obtained from the value NN using polyak averaging, i.e. after an update step the new target NN weights are calculated as a weighted average of its (99%) and the value NN’s (1%) weights.

calculated by

$$F(\rho_{\text{final}}, \rho_T) = \langle 0|U_C \rho_T U_C^\dagger|0\rangle \quad (11)$$

due to the invariance of the fidelity under unitary transformations.

3.2 Agent Structure

The remaining task is to train the weights W of the NN, so that its output vector, used as the estimate $Q_W(s_k, a_k)$, is very close to Q_{true} . Training data samples are generated by performing the circuit generation for Haar-random target states. State sampling includes partially separable states as well, e.g. only m of all qubits might be entangled by a Haar-random m -qubit unitary, whereas the other qubits are in random single-qubit states. To avoid bias, the positions of qubits are then shuffled randomly. We utilise the ε -greedy algorithm for action sampling to facilitate exploration, i.e. with probability ε we choose random actions, otherwise the highest value (the greedy action) is selected. The vectors representing states s_k and s_{k+1} , actions a_k , and rewards r_k are stored in a replay buffer.

When updating the network, a batch of individual steps from all stored episodes is sampled from the replay buffer with uniform probability. This prevents the agent from focusing only on recently sampled training data. A simplified schematic depicting the remaining steps of the update procedure of the DDQN agent is given in Figure 4. As one can see, the sampled data is

used to calculate the update targets

$$Q_{\text{target}}(s_k, a_k) = r_k + \gamma Q_{W'}(s_{k+1}, \arg \max_a Q_W(s_{k+1}, a)) \quad (12)$$

where $Q_{W'}$ represents the output of the target NN with weight W' , which is a delayed copy of the action selection NN and is obtained by polyak averaging of W' and W . This improves training stability by smoothing out rapid changes in the state-action value targets Q_W . NN weights W are updated using Adam gradient descent on the loss

$$L_{\text{DQN}} = \frac{1}{|B|} \sum_B (Q_W(s, a) - Q_{\text{target}}(s, a))^2 \quad (13)$$

of a batch B .

On top of these standard protocols we have used the following procedures to improve training efficiency. Firstly, we added the possibility of prioritized exploration to the standard ε -greedy algorithm. In many states, some gates perform significantly worse than others, e.g. when an individual qubit is already separable. By adding prioritized explorations we make it less likely that these actions are sampled, but still keep a high exploration rate of interesting states, e.g. where the agent cannot distinguish between the efficacy of only two actions. Our implementation adds a chance to randomly sample from only the actions with the highest state-action value estimates.

Secondly, instead of starting with a low threshold T_F as dictated by our desired accuracy, we

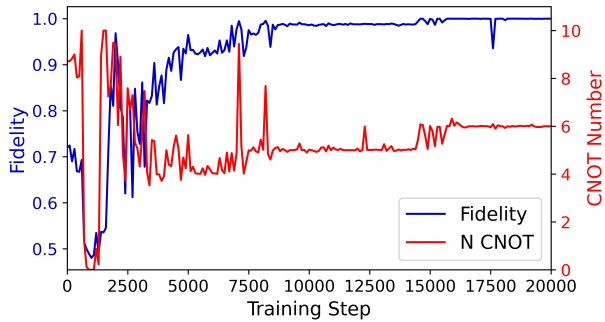


Figure 5: Performance on fully entangled Haar-random states over the course of training for a four-qubit system with unrestricted CNOT connectivity, i.e. all possible CNOT gates are available. The agent slowly improves fidelity by adding more CNOT gates, should they become necessary.

always use a high threshold to begin with and decrease it by exponential decay during training, if the agent is successful enough on the previous threshold. This is necessary, as when we train from scratch it is difficult to satisfy a high threshold by randomly guessing sequences.

Moreover, we have observed that adding information of previous actions to the input may result in the agent focusing too much on the action sequence and not considering the quantum state. By reducing the factor c_{in} from Eq. (5) in large infrequent steps after meeting the targeted threshold T_F , the agent is forced to focus more on ρ_k , leading to an adaptation of the gate sequence for individual target states.

4 Results

Training has been performed for systems with up to five qubits. Though only select architectures were tested, we expect the algorithm should converge to solutions for any, arbitrarily chosen, universal connectivity. Performance was evaluated by running the trained agents on a separate batch of 1000 Haar-random states. For this evaluation, we forgo exploration and have agents select greedy actions only, i.e. we set $\varepsilon = 0$. An example of the mean fidelity and number of CNOT gates used by the agent over the course of training can be seen in Figure 5. The latter is the main factor determining expressivity, thus more CNOT gates typically result in higher fidelities to the target state. Agents add gates if they are needed to match the threshold, but due to the penalty

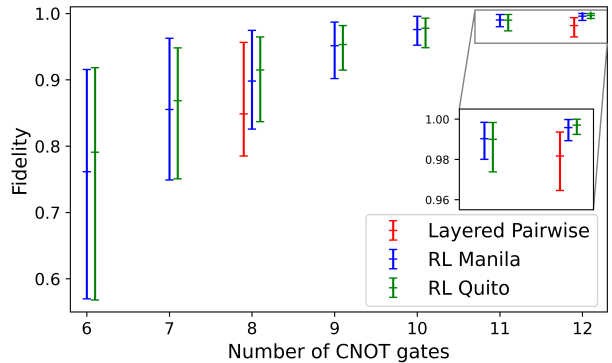


Figure 6: Performance of agents on different CNOT connectivities and of the pairwise hardware-efficient ansatz for a simulated five-qubit system without noise. Agents were restricted to fixed CNOT numbers, the exact x-value has been slightly shifted only for the visualization. NN agents have been limited to the systems connectivity. Layered approaches can only add full layers, thus less data points are available. Error bars depict the smallest interval containing 95% of the 100 total data samples.

from the discount factor, unnecessary gates are avoided.

Figure 6 compares agents against a hardware-efficient ansatz for an ideal system using the architecture of the `ibm_manila` and `ibm_quito` processors (see Figure 1). For the tested connectivities we are able to outperform the two layered circuit designs in Figure 2 at any number of layers, though we only show results for the pairwise architecture as it performed marginally better. Moreover, we can limit the maximally used number of CNOT gates by forcing the episodes to stop earlier in training and deployment. This may be especially beneficial for NISQ systems, as one can find a trade-off between the approximation error of a desired state and the noise introduced by adding more gates. The two depicted NN agents perform very similarly despite the difference in CNOT connectivity between `ibm_manila` and `ibm_quito`, demonstrating the adaptability of the approach. Figure 7 shows the importance of matching the experimental hardware. Even in the case that the circuit and hardware architecture differ in only one CNOT connection, one typically expects three extra CNOT gates to be added to circuits when using IBM’s built in transpiler. While more advanced transpilation and circuit optimization techniques exist, these can be computationally expensive or work best for non-universal gate sets (e.g. Clifford) or sparse

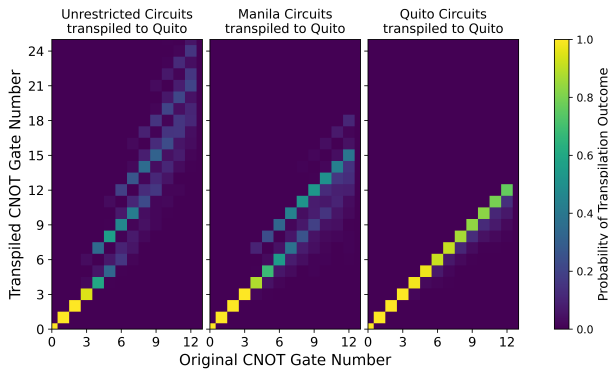


Figure 7: Effects of IBM transpiling with optimization level 3 on random single-qubit and CNOT gate sequences of varying length for five qubits on `ibm_quito`. Labeling above the circuit shows the connectivity layout from which the random circuit was generated. If the CNOT connectivity is not taken into account the CNOT gate number rises noticeably. At low gate counts, qubit relabeling can recover circuits that do not require gate replacement.

states. Thus they can struggle with arbitrary states, which we consider.

In order to verify that an actual advantage on experimental systems should be achievable we have tested our circuits on simulations of IBM quantum systems. The fidelities reached on `ibm_manila` and `ibm_quito` are depicted in Figure 8.

We have used the respective fake backends accessible through `qiskit`, which provide a past snapshot with noise parameters measured on the actual device. To reconstruct the density matrix ρ and calculate the fidelity to the target state, we perform a full quantum state tomography with maximum likelihood estimation [42]. Readout errors were discarded from the simulation, because our focus lies only on improving the circuit gate sequence, however this should not affect our overall conclusions. On an actual physical device one has to use readout error mitigation techniques instead [14].

The most immediate observation is that significantly better fidelities are achieved on `ibm_manila` in general. This is due to lower gate errors and longer dephasing and relaxation times. Though it should be noted that for `ibm_quito` we typically observed higher fidelities on the physical device than in simulations. This can be seen in Table 1 comparing previous runs between the real and simulated versions for `ibm_quito` with only local optimization. When simulating

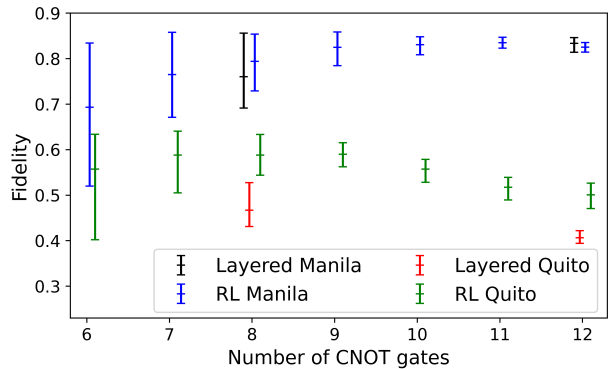


Figure 8: Performance of agents on noisy simulations of IBM backends with readout error disabled. Visualization analogous to Fig. 6. One can clearly see that using the RL agents we reach optimal performance below 12 CNOT gates. On `ibm_manila` the RL agent and layered circuit perform quite similarly though our approach allows for arbitrary CNOT number. For `ibm_quito`, which is more impacted by noise in general, there is also a drastic difference between the RL agent and layered circuit due to transpiling effects.

Type	real	sim	sim
Optimizer	local	local	global
Mean Fidelity	0.693	0.56	0.594
Interval	± 0.053	± 0.12	± 0.019

Table 1: Comparison of performance on real device and in simulation for `ibm_quito`, including measurement noise. Means and error bars are obtained over 78 four-qubit Haar-random target states. For `ibm_quito` the real device results are much better than the simulation. We assume that the difference is caused by the noise parameters of the device snapshot used for the simulator. One can see that the global optimizer is noticeably better than the local optimizer for simulated results. A similar improvement should be expected for real device results.

`ibm_quito` and using the global optimizer (see Figure 8), we can observe a maximum in the mean fidelity attained by the RL agent at 9 CNOT gates. For `ibm_manila` the fidelity peaks at 11 CNOT. This difference can also be understood as a result of noise: As each gate incurs a bigger penalty with increasing noise, the optimum between the approximation error and circuit noise shifts in favour of higher allowable approximation errors. Performance of the layered circuit differs markedly between the experimental devices. While on `manila` it is close to the RL agent, on `quito` the necessity of inserting additional CNOT gates during transpiling results in a significant drop in fidelity.

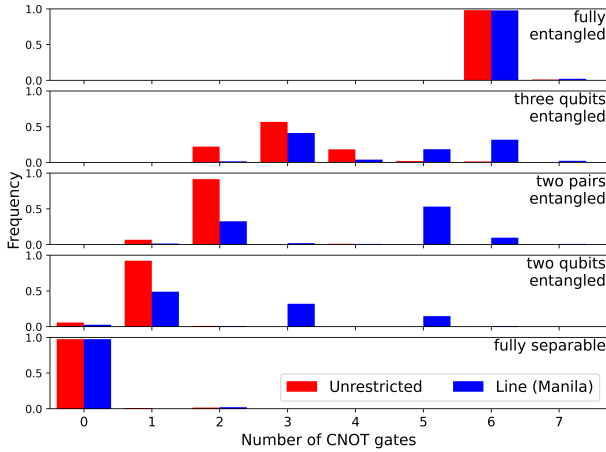


Figure 9: Frequency of the number of applied CNOT gates over 1000 states for each entanglement structure. The "Unrestricted" data points are from an RL agent with all CNOT connections available, the "Line" agent only has connections to the nearest qubits by index. To create states for each separable subsystem Haar random unitaries are sampled. Qubit positions were shuffled. Depicted agents generate circuits with above 0.999 mean fidelity to the target. The Line agent requires more gates if the entangled qubits are separated with respect to its connectivity.

We have also investigated the performance of our trained agents for separable states on four-qubit systems (see Fig. 9). Here, results of agents with restricted connectivities may differ significantly from those of agents with full qubit connectivity. For example, a two-qubit entangled state can only be reached using a single CNOT if the direct connection is part of the gate set. For short circuits a relabeling step can circumvent this problem.

In order to guarantee that agents can learn to adapt to individual targets, we have checked their performance on well-known fully entangled states with proven optimal implementations. Specifically, this was done for the GHZ-state and W-state. The four-qubit agents correctly identify circuits with a lower number of entangling gates when compared to a random target, demonstrating that the agent is not just using highly expressive circuits. This is remarkable, as the GHZ-state and W-state were almost certainly never observed directly in the training data. On 10 datasets containing 2 million Haar random states each, we observed a maximum fidelity to a W- or GHZ-state of around 0.678. We estimate a probability of less than 0.1% that the highest fidelity to the W-state or GHZ-state in a training

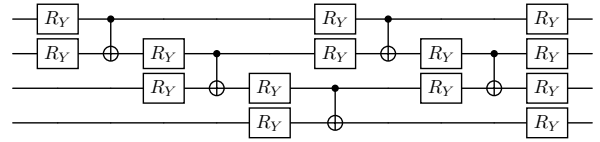


Figure 10: Circuit found by the RL agent for the four-qubit W-state that may be generalized to n qubits.

Number of CNOT	Optimal Fidelity	RL Example Sequence
3	0.8	2-3, 1-2, 0-2
4	0.933	1-2, 2-3, 1-0, 1-2
5	1	0-1, 1-2, 2-3, 2-1, 1-0

Table 2: Performance on four-qubit W-states with example circuits extracted from RL. The listed sequence written as a list of gates with each gate in the format "control-target".

set was above 0.75. For GHZ states the number of employed entangling gates is equal to the known optimal gate number of $n - 1$, i.e. three CNOTs on four qubits. For W-states, accurate circuits containing only five CNOT were found. The general structure for the four-qubit W-state circuit (see Figure 10) can be generalized to arbitrary n and requires only $2(n - 1) - 1$ CNOTs. We have tested for up to ten qubits that these circuits accurately create the W-state. However, a general expression for the rotation gate angles eludes us.

Agents with thresholds allowing for lower approximation accuracy adjust the gate number to match the target requirements. Circuits remained optimal when restricting the available resources in this way, which we have verified through brute-forcing (see Table 2).

5 Conclusion

We have demonstrated an algorithm that is capable of finding quantum gate sequences for arbitrary target states, generating them with a higher fidelity than layered parameterized quantum circuits. Tuning the CNOT gate number or threshold allows us to set the approximation accuracy and balance it with respect to experimental noise. For five qubits it was consistently possible to train to above 0.99 mean fidelity to random target states in simulations. We expect that, experimentally, our approach will allow for higher state

preparation fidelity, especially on systems dominated by entangling gate noise. Combining our algorithm with other circuit optimization protocols could yield even better results.

The biggest advantage of our approach is its flexibility and tunability. RL promises to work regardless of the gate set or qubit connectivity. Furthermore, one can choose desired target thresholds for the training, giving the ability to find a trade-off between minimizing experimental noise and approximation error.

Compared to previous RL methods, which were mostly designed for gate sets without continuous parameters, such as the Clifford set or the Toffoli+T gate set, we expect an improvement in the direct applicability to experimental devices with low qubit numbers. The Clifford gate set is not universal, and discrete gate sets are likely to be inefficient in terms of gate number or depth, because for operations which are easily achieved by few continuous parameters they necessitate long chains of discrete gates. However, a potential drawback of our method is the limitation to smaller qubit numbers than non-universal approaches, as the proposed algorithms requires information of the quantum state as input and needs to simulate the state evolution to gather training data. With future development, one may be able to deal with these issues by using an accurate but unoptimized gate sequence as input and by obtaining training data from real NISQ quantum computers. The latter would also immediately give access to the exact noise behaviour.

6 Acknowledgments

We acknowledge the use of IBM Quantum services for this work. The views expressed are those of the authors, and do not reflect the official policy or position of IBM or the IBM Quantum team. This work was partially financially supported by the Deutsche Forschungsgemeinschaft via the International Research Training Group 2676 'Imaging quantum systems (IQS): photons, molecules, materials', grant no. 437567992.

References

- [1] Qingling Zhu et al. "Quantum computational advantage via 60-qubit 24-cycle random circuit sampling". *Science Bulletin* **67**, 240–245 (2022).
- [2] Lars S. Madsen et al. "Quantum computational advantage with a programmable photonic processor". *Nature* **606**, 75–81 (2022).
- [3] A. Morvan et al. "Phase transitions in random circuit sampling". *Nature* **634**, 328–333 (2024).
- [4] Sergio Boixo et al. "Characterizing quantum supremacy in near-term devices". *Nature Physics* **14**, 595–600 (2018).
- [5] P.W. Shor. "Algorithms for quantum computation: discrete logarithms and factoring". In Proceedings 35th Annual Symposium on Foundations of Computer Science. Pages 124–134. (1994).
- [6] Thomas Monz et al. "Realization of a scalable shor algorithm". *Science* **351**, 1068–1070 (2016).
- [7] Francesco Tacchino, Alessandro Chiesa, Stefano Carretta, and Dario Gerace. "Quantum computers as universal quantum simulators: State-of-the-art and perspectives". *Advanced Quantum Technologies* **3**, 1900052 (2020).
- [8] David Peral-García, Juan Cruz-Benito, and Francisco José García-Peñalvo. "Systematic literature review: Quantum machine learning and its applications". *Computer Science Review* **51**, 100619 (2024).
- [9] Rajeev Acharya et al. "Quantum error correction below the surface code threshold". *Nature* (2024).
- [10] John Preskill. "Quantum Computing in the NISQ era and beyond". *Quantum* **2**, 79 (2018).
- [11] Olivia Lanes et al. "A framework for quantum advantage" (2025). [arXiv:2506.20658](https://arxiv.org/abs/2506.20658).
- [12] Youngseok Kim et al. "Evidence for the utility of quantum computing before fault tolerance". *Nature* **618**, 500–505 (2023).
- [13] Javier Robledo-Moreno et al. "Chemistry beyond the scale of exact diagonalization on a quantum-centric supercomputer". *Science Advances* **11**, eadu9991 (2025).
- [14] Zhenyu Cai et al. "Quantum error mitigation". *Rev. Mod. Phys.* **95**, 045005 (2023).
- [15] Gabriel Popkin. "Quest for qubits". *Science* **354**, 1090–1093 (2016).
- [16] Ali Javadi-Abhari et al. "Quantum computing with qiskit" (2024). [arXiv:2405.08810](https://arxiv.org/abs/2405.08810).

- [17] Fei Hua et al. “Qasmtrans: A qasm quantum transpiler framework for nisq devices”. In Proceedings of the SC ’23 Workshops of The International Conference on High Performance Computing, Network, Storage, and Analysis. Page 1468–1477. SC-W ’23 New York, NY, USA (2023). Association for Computing Machinery.
- [18] John van de Wetering and Matt Amy. “Optimising quantum circuits is generally hard” (2024). [arXiv:2310.05958](https://arxiv.org/abs/2310.05958).
- [19] John van de Wetering, Richie Yeung, Tuomas Laakkonen, and Aleks Kissinger. “Optimal compilation of parametrised quantum circuits”. *Quantum* **9**, 1828 (2025).
- [20] M. Cerezo et al. “Variational quantum algorithms”. *Nature Reviews Physics* **3**, 625–644 (2021).
- [21] Abhinav Kandala et al. “Hardware-efficient variational quantum eigensolver for small molecules and quantum magnets”. *Nature* **549**, 242–246 (2017).
- [22] Jules Tilly et al. “The variational quantum eigensolver: A review of methods and best practices”. *Physics Reports* **986**, 1–128 (2022).
- [23] Marcello Benedetti, Erika Lloyd, Stefan Sack, and Mattia Fiorentini. “Parameterized quantum circuits as machine learning models”. *Quantum Science and Technology* **4**, 043001 (2019).
- [24] Amira Abbas, David Sutter, Christa Zoufal, Aurelien Lucchi, Alessio Figalli, and Stefan Woerner. “The power of quantum neural networks”. *Nature Computational Science* **1**, 403–409 (2021).
- [25] Adriano Barenco et al. “Elementary gates for quantum computation”. *Phys. Rev. A* **52**, 3457–3467 (1995).
- [26] Ville Bergholm, Juha J. Vartiainen, Mikko Möttönen, and Martti M. Salomaa. “Quantum circuits with uniformly controlled one-qubit gates”. *Phys. Rev. A* **71**, 052330 (2005).
- [27] Martin Plesch and Āaslav Brukner. “Quantum-state preparation with universal gate decompositions”. *Phys. Rev. A* **83**, 032302 (2011).
- [28] Xiao-Ming Zhang, Tongyang Li, and Xiao Yuan. “Quantum state preparation with optimal circuit depth: Implementations and applications”. *Phys. Rev. Lett.* **129**, 230504 (2022).
- [29] Sukin Sim, Peter D. Johnson, and Alán Aspuru-Guzik. “Expressibility and entangling capability of parameterized quantum circuits for hybrid quantum-classical algorithms”. *Advanced Quantum Technologies* **2**, 1900070 (2019).
- [30] Yuxuan Du, Min-Hsiu Hsieh, Tongliang Liu, and Dacheng Tao. “Expressive power of parametrized quantum circuits”. *Phys. Rev. Res.* **2**, 033125 (2020).
- [31] Florian Fūrrutter, Gorka Muñoz-Gil, and Hans J. Briegel. “Quantum circuit synthesis with diffusion models”. *Nature Machine Intelligence* **6**, 515–524 (2024).
- [32] David Kremer, Victor Villar, Hanhee Paik, Ivan Duran, Ismael Faro, and Juan Cruz-Benito. “Practical and efficient quantum circuit synthesis and transpiling with reinforcement learning” (2024). [arXiv:2405.13196](https://arxiv.org/abs/2405.13196).
- [33] Sebastian Rietsch et al. “Unitary synthesis of clifford+t circuits with reinforcement learning”. In 2024 IEEE International Conference on Quantum Computing and Engineering (QCE). Volume 01, pages 824–835. (2024).
- [34] Jordi Riu, Jan Nogué, Gerard Vilaplana, Artur Garcia-Saez, and Marta P. Estarellas. “Reinforcement Learning Based Quantum Circuit Optimization via ZX-Calculus”. *Quantum* **9**, 1758 (2025).
- [35] Francisco J. R. Ruiz et al. “Quantum circuit optimization with alphasensor”. *Nature Machine Intelligence* **7**, 374–385 (2025).
- [36] A Yu Kitaev. “Quantum computations: algorithms and error correction”. *Russian Mathematical Surveys* **52**, 1191 (1997).
- [37] Michael A. Nielsen and Isaac L. Chuang. “Quantum computation and quantum information: 10th anniversary edition”. Cambridge University Press. (2010).
- [38] James Stokes, Josh Izaac, Nathan Killoran, and Giuseppe Carleo. “Quantum Natural Gradient”. *Quantum* **4**, 269 (2020).
- [39] Hado van Hasselt, Arthur Guez, and David Silver. “Deep reinforcement learning with double q-learning”. *Proceedings of the AAAI Conference on Artificial Intelligence*, **30** (2016).
- [40] Tom Rieckmann and A. Douglas K. Plato.

- “Gate Sequence Optimization for Parameterized Quantum Circuits using Reinforcement Learning”. <https://github.com/Arphobor/QCOptim.git> (2025).
- [41] Christopher M. Bishop and Hugh Bishop. “Deep learning: Foundations and concepts”. Page 226. Springer International Publishing. (2023).
- [42] Zdeněk Hradil, Jaroslav Řeháček, Jaromír Fiurášek, and Miroslav Ježek. “Quantum state estimation”. Springer Berlin, Heidelberg. (2004).